Supplementary Information

Achieving Strong and Reliable Underwater Adhesive Based on A Simple and Generic Amino-Acid-Resembling Design

Feng Li [1], Jiaying Mo [2], Zhicheng Zhang [1], Sheldon. Q. Shi [3], Jianzhang Li [1], Jinfeng Cao [1]*, Zuankai Wang [4]**

[1] MOE Key Laboratory of Wood Material Science and Application & Beijing Key Laboratory of Wood Science and Engineering, Beijing Forestry University, Beijing 100083, China

[2] Department of Mechanical Engineering, City University of Hong Kong, Hong Kong, China
Hong Kong Centre for Cerebro-Caradiovasular Health Engineering (COCHE), Hong Kong 999077, China

[3] Department of Mechanical and Energy Engineering, University of North Texas, Denton, TX 76203, USA

[4] Department of Mechanical Engineering, The Hong Kong Polytechnic University, Hong Kong, China

* Corresponding author Email: lijzh@bjfu.edu.cn (J. Li), CJF940204@bjfu.edu.cn (J. C), and zuanwang@polyu.edu.hk (Z. W)

EXPERIMENTAL METHODS

Materials

Octaglycidyloxypropyl-silsesquioxane (Glycidyl-POSS, GP) was purchased from Xi'an Qiyue Biological Technology Co., Ltd. (Xi'an, China). 2-Amino-5-mercapto-1,3,4-thiadiazole (AMTD), 2-Amino-1,3,4-thiadiazole (ATD), cyclopentylamine (CPA), 3-Amino-5-mercapto-1,2,4-triazole (AMT), 5-Amino-2-mercaptobenzimidazole (AMBD), 2-Amino-benzothiazol-6-ol (ABTO), N, N-Diglycidyl-4-glycidyloxyaniline (DGLA) and bis(2,3-epoxypropyl) cyclohex-4-ene-1,2-dicarboxylate (BCED) were obtained from Aladdin Biochemical Technology Co., Ltd (Shanghai, China). Sorbitol polyglycidyl ether (SPGE) was obtained from Wuhan Huaxiang Kejie Biotechnology Co., Ltd. Sea salt was obtained from Shandong Bessen Feed Co., Ltd. Hydrochloric acid (HCl), sodium hydroxide (NaOH), and ethanol were provided by Sinopharm Chemical Reagent Co., Ltd (Beijing, China). All chemicals were used as received without further purification. Commercial underwater adhesives (epoxy, polyurethane, and silane modified polyether adhesives) for adhesion comparison were purchased from Dongguan HUIERGILUE Sealing Adhesive Co., Ltd. (Dongguan, China), Minnesota Mining and Manufacturing (3M) Company (United States), and Guangdong Evergrande New Material Technology Co., Ltd. (Guangdong, China), respectively.

Preparation of AARA

The AARAs were prepared by a one-step and solvent-free method. In brief, 1 mol GP liquid and AMTD powder with specific molar ratio (e.g. 0, 2.5, 4, 5, and 6.25, related to the molar of GP) were mixed and stirred for 5 min at ambient temperature, finally yielding a white sticky adhesive precursor. Upon applying in water, adhesive precursor can spontaneously solidify into the resultant AARA. Unless otherwise specified, AARA denotes the GP/AMTD combination with a 4 molar ratio of AMTD (relative to GP) because of its optimal adhesion performance. Other AARAs including GP/AMT, GP/AMBD, GP/ABTO, SPGE/AMTD, DGLA/AMTD, and BCED/AMTD adhesives were fabricated with the same method to GP/AMTD combination.

Surface contact angle (CA)

The contact angles were measured at room temperature using an OCA20 contact angle analyzer (Dataphysics Instruments GmbH, Filderstadt, Germany). For the contact angles of water droplets on adhesive surface, the fabricated AARA was applied on glass substrate, and then distilled water was dropped in air condition. For the contact angles of adhesive droplets on glass surface, AARA was dropped on a glass substrate in water condition.

Fourier transform infrared (FTIR) spectrometry

The Fourier transform infrared (FTIR) spectra were recorded using the attenuated total reflectance (ATR) method (Nicolet 6700, Thermo Scientific, USA) within the wavenumber range of 500 to 4000 cm^{-1} with 32 scans. The conversion of epoxy groups can be determined by

$$C = (A_0 - A_t)/A_0 \times 100\% \ ^{1},$$

where A_0 and A_t are the normalized peak areas of epoxy (907 cm^{-1}) with respect to methyl (2936 cm^{-1}) before and after curing at time t, respectively.

Rheology measurement

The rheological properties of AARA were obtained using a rotary rheometer (Anton Paar, MCR301) equipped with a flat parallel plate (25 mm in diameter) at 25℃. An oscillatory frequency sweep of the samples was carried out over the frequency range 0.1 to 100 rad/s with γ = 1% at a fixed strain amplitude. For the strain sweeping experiments, all samples were performed under a constant shear rate of 10 rad/s, with the strain range 0.1 to 100%. The distance was set to 1 mm throughout the measurements.

Differential scanning calorimetry (DSC) measurements

DSC analysis was carried out on a DSC apparatus (Q2000, TA Instruments). Heating and cooling rates of 20 ℃/ min were used over the temperature range of −80 to 80 ℃.

Low-field ^{1}H NMR (LF ^{1}H NMR) measurement

LF ^{1}H NMR measurements were performed at 32 °C on a 21 MHz NMR Analyzer (VTMR20-010V-I, Niumag Corporation Ltd., Shanghai, China). Carr-Purcell-Meiboom-Gill (CPMG) sequences were employed to measure spin-spin relaxation time

(T_2) to collect decay signals. T_2 measurements were performed with 18000 echoes recorded for each transient, an inter-echo interval of 100 μs, a recycle time of 10000 ms, and a total of 8 added transients. The pulse durations were 2.80 and 5.44 μs for the 90° and 180° pulses, respectively.

X-ray photoelectron spectrometry (XPS)

The chemical compositions of AMTD and AARA were measured by an X-ray photoelectron spectrometer (XPS, ESCALAB 250XI, Thermo, England) with a binding energy range of 0–1200 eV.

Molecular dynamics (MD) simulation

To study the underwater adhesion mechanism of AARA, AMTD and its two analogues (ATD and CPA) were used for comparison. The all-atom molecular dynamics (MD) simulations were conducted to calculate the adhesion systems by using the Materials Studio software program.

For the bulk adhesive, three different molecular models (AARA, GP/ATD and GP/CPA combinations) were built to evaluate their structure characters. Each model contains 8 GP backbones and 32 functional blocks (AMTD, ATD, or CPA). The final crosslink degree of adhesive network is calculated by FTIR results (see Table S1). A series of mechanical properties, including bulk modulus, shear modulus, and Young's modulus, were calculated by MD simulation using the Voigt–Reuss–Hill approach.

For the interfacial adhesion between adhesive and glass substrate in water, the molecular model of the interaction between adhesive and surface was established. Firstly, the glass substrate was modeled by a periodically repeated SiO_2 (001) layers with hydroxylated surface, and the constructed size was 34.4×34.0×12.8 Å. Then, to better simulate the adhesion behavior in water, an interface adhesive model was established by five-layers consisting of vacuum slab, bulk water layer, adhesive layer, interfacial water layer, and glass substrate (see Fig. S10).

The force field of Condensed-phase Optimized Molecular Potential for Atomistic Simulation Studies (COMPASS II) was adopted in this study. The COMPASS force field was commonly used to provide the atomic interactions. Van der Waals interactions were treated using an atom-based cut-off method with a cut-off of 12.5 Å, and the

Coulomb interactions were calculated by the Ewald summation method with an accuracy of 10^{-3} kcal mol^{-1}. To obtain a reasonable interaction configuration between the adhesive and glass surface, a geometry optimization using smart method with an energy convergence criterion of 1×10^{-5} kcal mol^{-1} and force convergence criteria of 0.5 kcal mol^{-1} $Å^{-1}$ were used to get a global minimum energy configuration. Then, an equilibrate process was followed under constant temperature and constant volume (NVT ensemble) at 298 K for 1000 ps with a time step of 1 fs. Andersen thermostat was applied for the temperature control. During the simulation process, the water molecules on the glass surface were gradually removed with more close interfacial bonding. The interaction energy between adhesive and glass substrate was calculated by the following formula:

$$E_{interfacial} = E_{total} - (E_{adhesive} + E_{substrate})$$

where, $E_{interfacial}$ represents the interaction energy between adhesive and surface. $E_{adhesive}$ and $E_{substrate}$ are the potential energies of adhesive and glass surface, respectively. E_{total} indicates the total potential energy of the model system. The larger the negative E_{total}, the stronger the interaction.

Measurement of adhesion strength

A lap-shear strength test was conducted using a universal testing machine with 10 kN load-cell (INSTRON 3365, Norwood, MA, USA). For the evaluation of adhesion strength, six different substrates: wood, steel, poly(vinyl chloride) (PVC), poly(methyl methacrylate) (PMMA), glass, poly(tetrafluoroethylene) (PTFE), were selected and prepared with a size of 80 mm × 25 mm × 2 mm. Prior to the test, the substrates were cleaned with ethanol and deionized water, and then completely dried at room temperature. The underwater adhesion process was conducted in pure water at room temperature. The adhesive was applied uniformly to the surface of one substrate with a bonding area of 25 mm × 25 mm under the submerged condition to bind with the another one substrate. For glass substrate, the overlapped area was set as 25 mm × 5 mm due to its fragility. The adhered substrates were pressed by hand to ensure intimate contact (the adhesion thickness is about 0.2 mm), and stored in water for different durations (0 h, 12 h, 24 h, 36 h, 48 h, 72 h, and 1 month). It is noted that a 30 g weight

is applied on the glued wood plates during the immersion to prevent to float on the water. Similarly, the adhesion strengths were measured for the samples in different aqueous environments (pH = 3, pH = 10, 50 ℃, 80 ℃, and seawater solutions) and non-aqueous solution (absolute ethanol). Each sample was removed from the solution and immediately subjected to a lap-shear test to measure its adhesion strength at a controlled rate (20 mm/min). The average adhesive strengths were calculated from the maximum force at failure divided by the overlap area based on five replicates. The adhesion strengths of commercial adhesives were tested according with the above method. Unless otherwise specified, the adhesion strengths of adhesives were tested after immersing 48 h in solutions.

Artificial seawater was prepared by dissolving sea salt (1 kg) in deionized water (30 kg). Acid and alkali aqueous solutions were adjusted with HCl and NaOH to pH = 3 and pH = 10, respectively. High-temperature water solutions (T = 50 and 80 ℃) were heated in a water bath (HWS-12, Shanghai Yiheng Scientific Instrument Co., Ltd.).

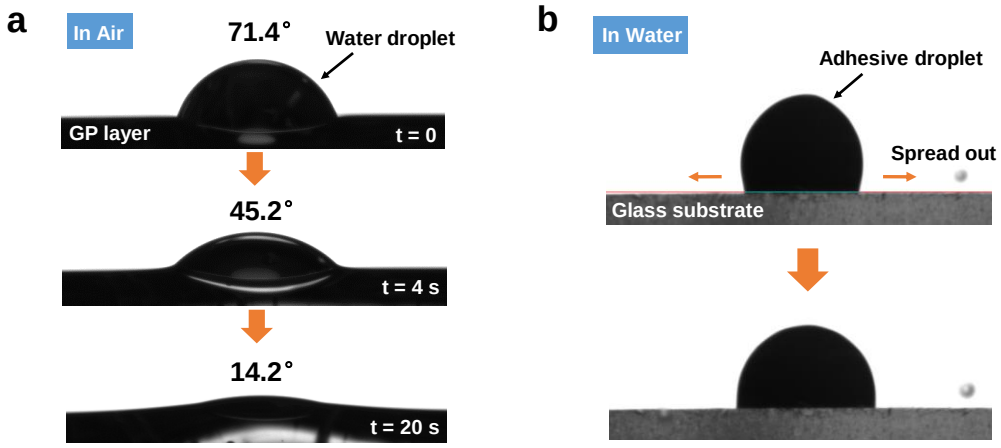

Fig. S1. Surface contact angle images of (a) the water droplet to GP layer in air and (b) the adhesive precursor droplet to glass substrate in water.

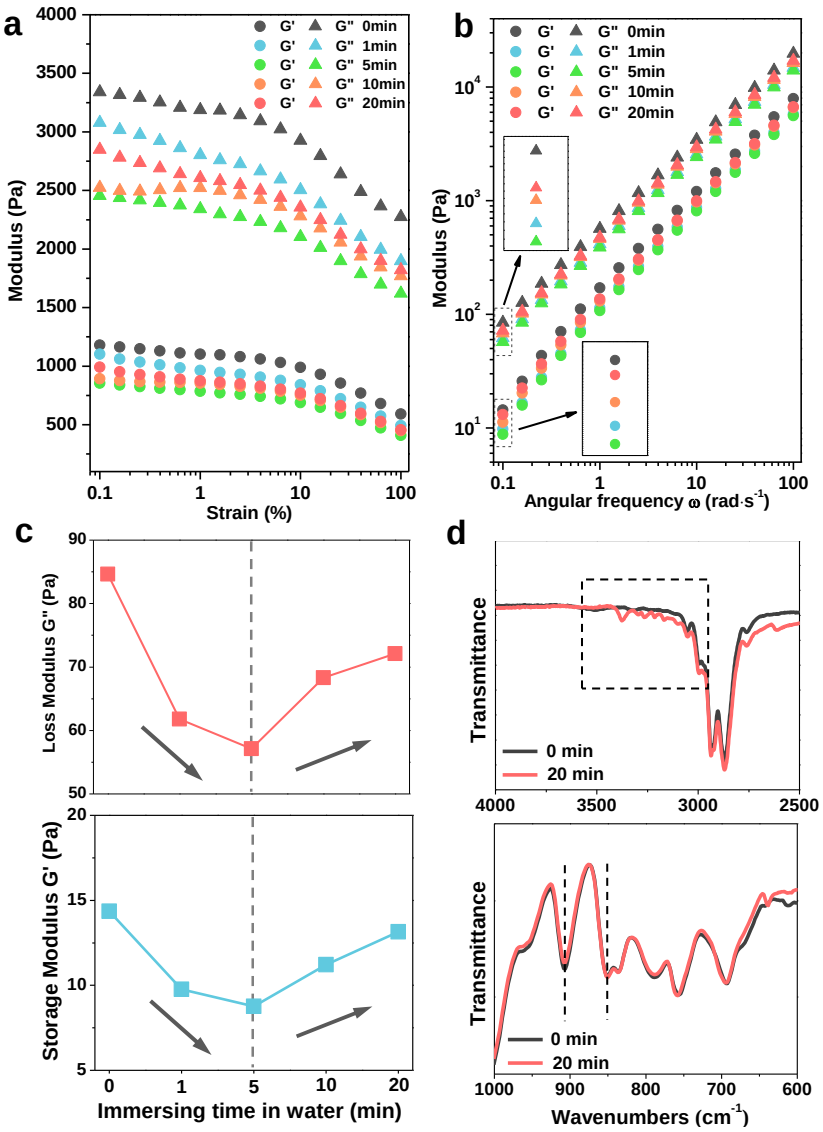

Fig. S2. Rheological tests of adhesive precursors (a) for the strain sweep (angular frequency = 10 rad s^{-1}, strain = 0.1-100 %), and (b) for the angular frequency sweep (strain = 1%, angular frequency = 0.1-100 rad s^{-1}) with different immersing time in water. (c) The modulus values of AARAs with different immersing time in water (strain = 1%, frequency = 0.1 rad s^{-1}). (d) ATR–FTIR spectra of adhesives with different immersing time in water. It is noted that the samples were lyophilized before FTIR measurements.

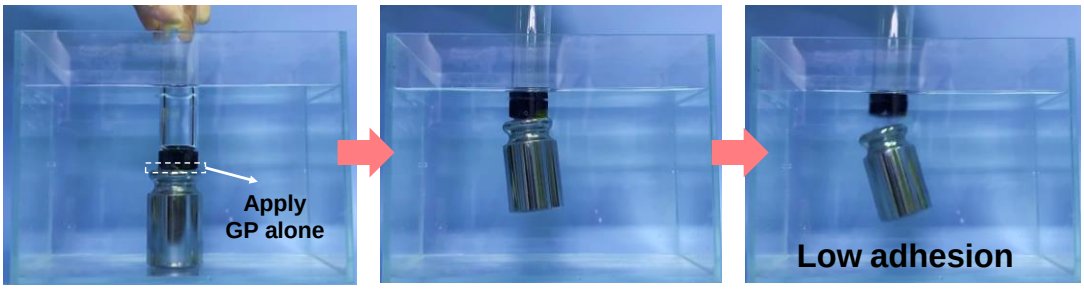

Fig. S3. Digital images showing the poor underwater adhesion capability of GP liquid.

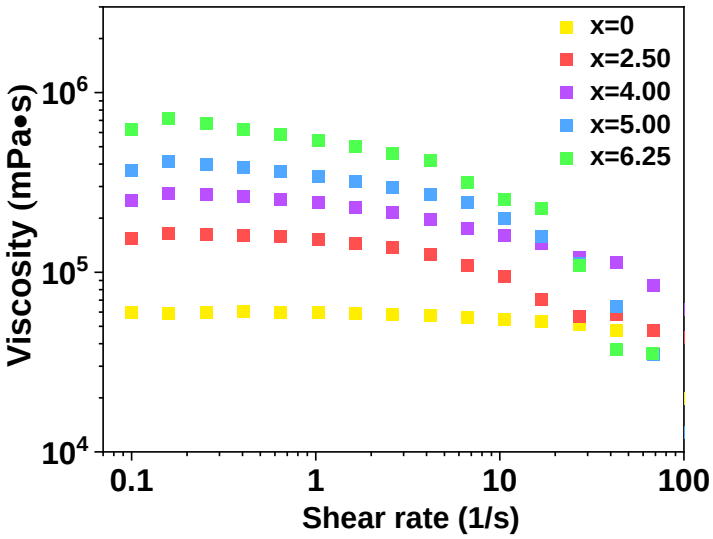

Fig. S4. Viscosity of adhesive precursors at various AMDT molar ratio (*x*, relative to the molar of GP).

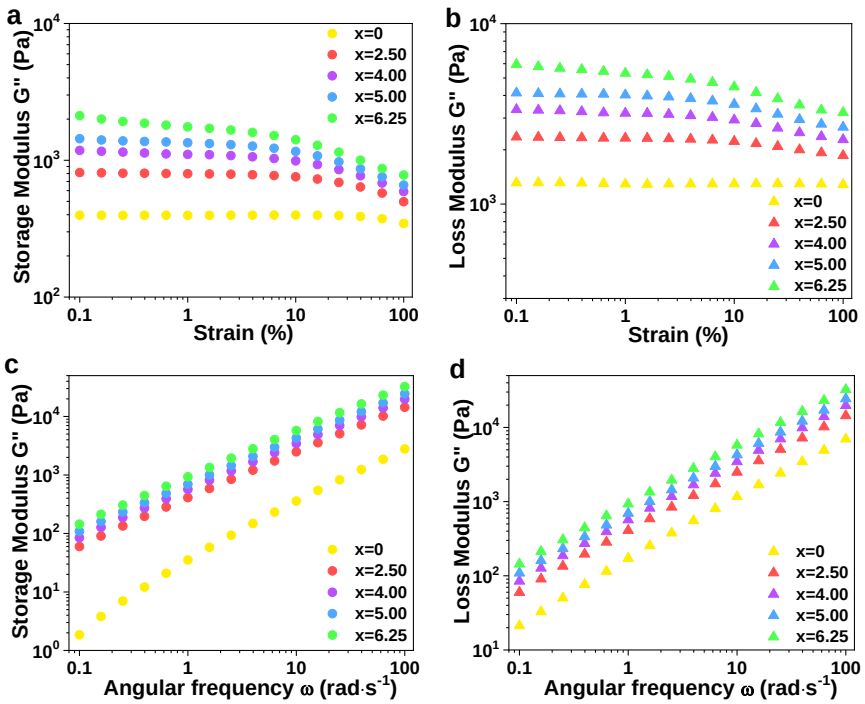

Fig. S5. Rheological tests of adhesive precursors at various *x* (a, b) for the strain sweep (angular frequency = 10 rad s^{-1} and strain = 0.1-100 %), and (c, d) for the angular frequency sweep (strain = 1% and angular frequency = 0.1-100 rad s^{-1}).

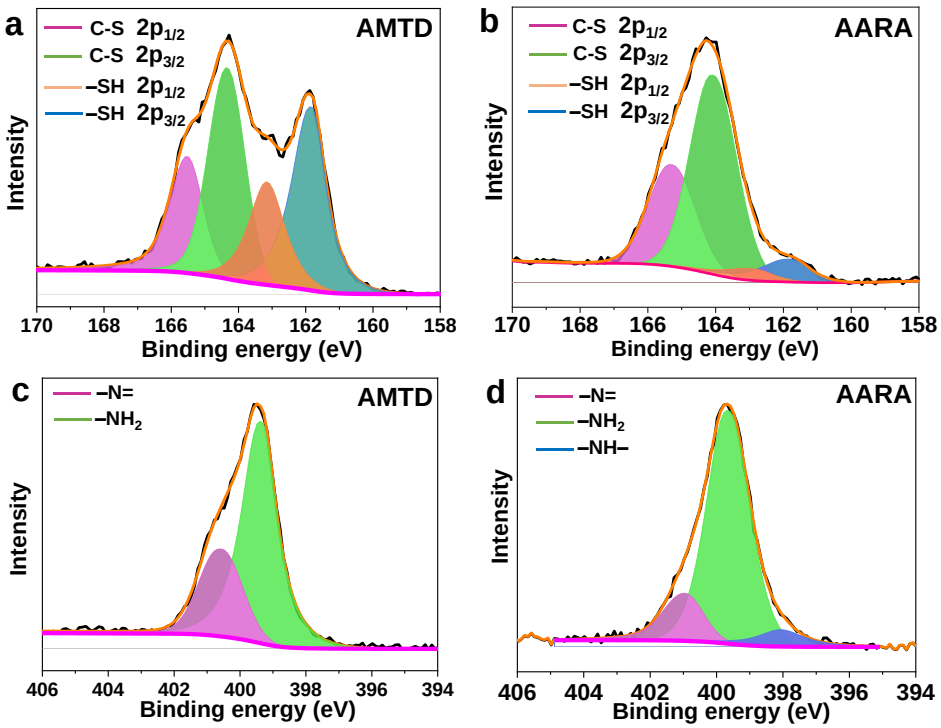

Fig. S6. Peak-fitting XPS spectra in the S 2p regions of (a) AMTD and (b) underwater-cured AARA. Peak-fitting XPS spectra in the N 1s regions of (c) AMTD and (d) underwater-cured AARA.

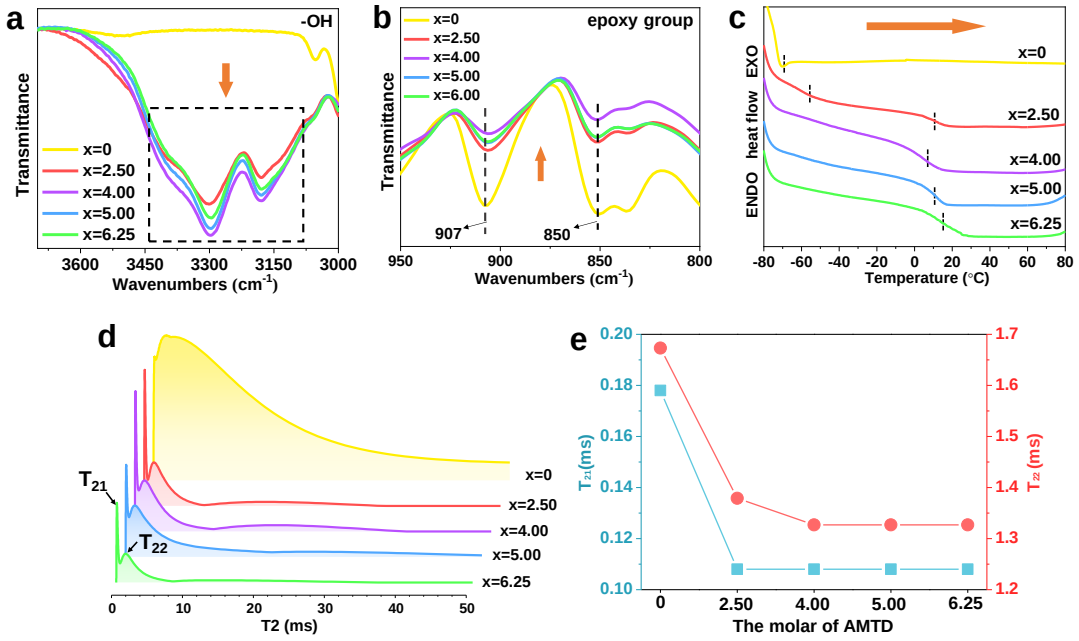

Fig. S7. (a, b) ATR–FTIR spectra, (c) DSC curves, (d) Low-field ^{1}H NMR spectra and (e) the corresponded relaxation time (T_2) value of the cured AARAs with various *x* in water (t = 48 h). It is noted that a lower T_2 value indicates the more restricted molecular chain.

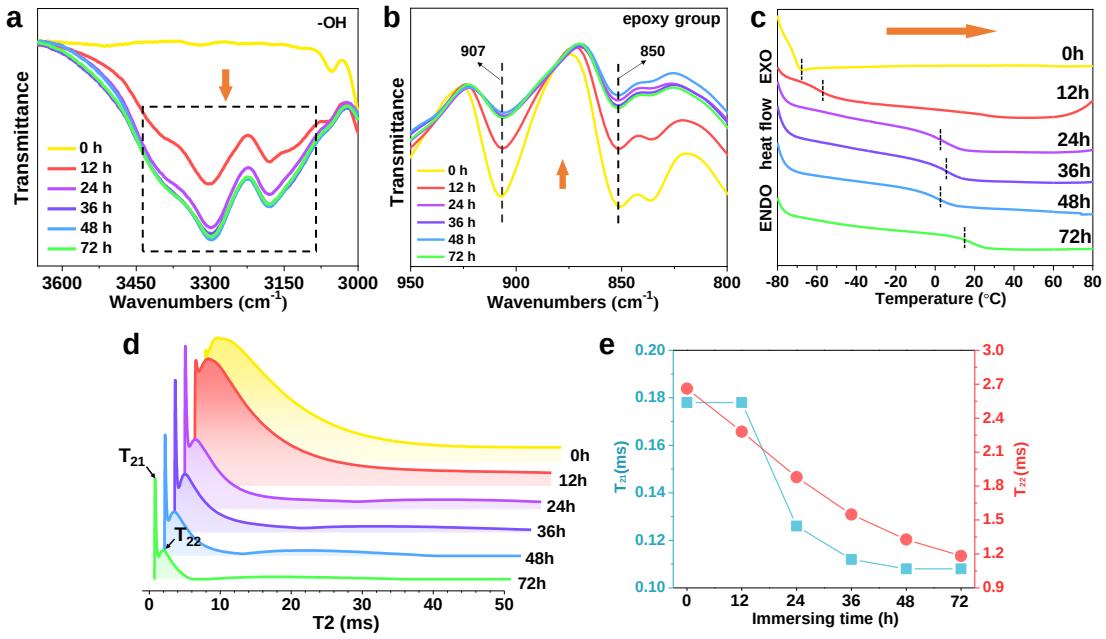

Fig. S8. (a, b) ATR–FTIR spectra, (c) DSC curves, (d) Low-field ^{1}H NMR spectra and (e) the corresponded relaxation time (T_2) value of the cured AARAs ($x = 4$) with various immersing time in water.

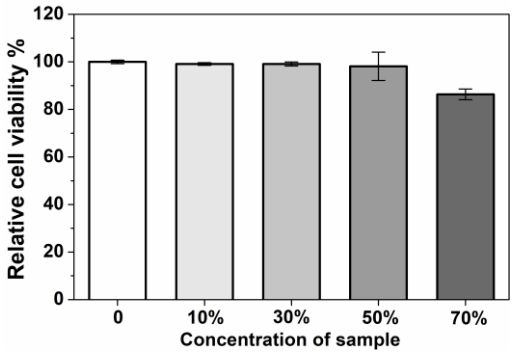

Fig. S9. The activity of NIH-3T3 cells in co-culture with AARA samples for 48 h.

Cell Counting Kit-8 (CCK-8) assays were used to examine cell viability. Briefly, the UV-irradiated sterilized cured adhesive was soaked in complete DMEM medium for 24 h (surface area of sample: extraction solution = 1.25 cm^2: 1 mL), and then extracted 0.22 μm solution. The complete DMEM medium was used to configure adhesive extracts with concentrations of 0%, 10%, 30%, 50%, and 70%, respectively. NIH 3T3 cells were cultured at 2×10^4 cells per well in 96-well plates for 24 h. After replacing the original medium with different concentrations of extracts, the culture was continued for 48 h. The 100μL respective cell culture medium containing 10% CCK-8 was added to each well of 96 orifice plate. The CCK-8 solution was collected after 2 h in a dark environment. The absorbance at 450 nm was recorded immediately on a microplate reader.

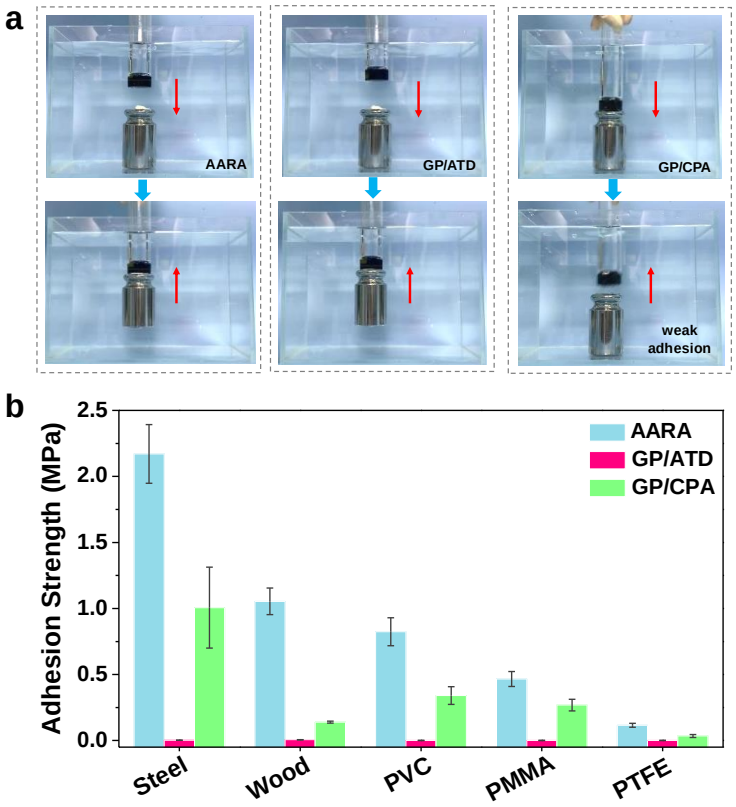

Fig. S10. Adhesion images of (a) AARA, GP/ATD, and GP/CPA adhesives to 500 g weight under water. (b) Lap-shear underwater adhesion strengths of AARA, GP/ATD, and GP/CPA adhesives under water.

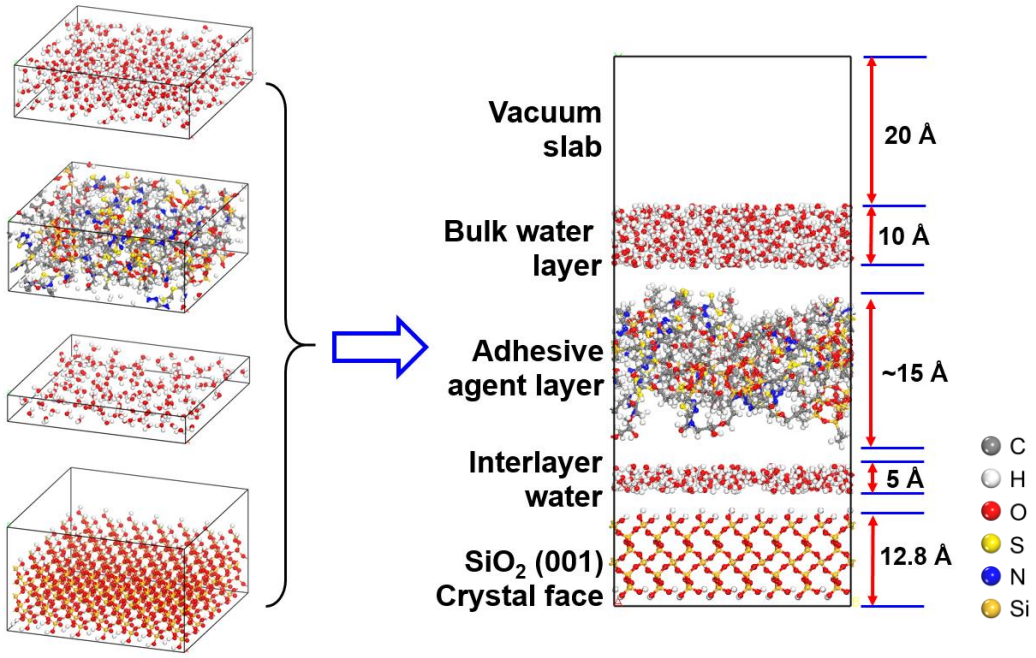

Fig. S11. Schematic illustration of the MD simulation model for the interfacial adhesion between adhesive and glass substrate under water

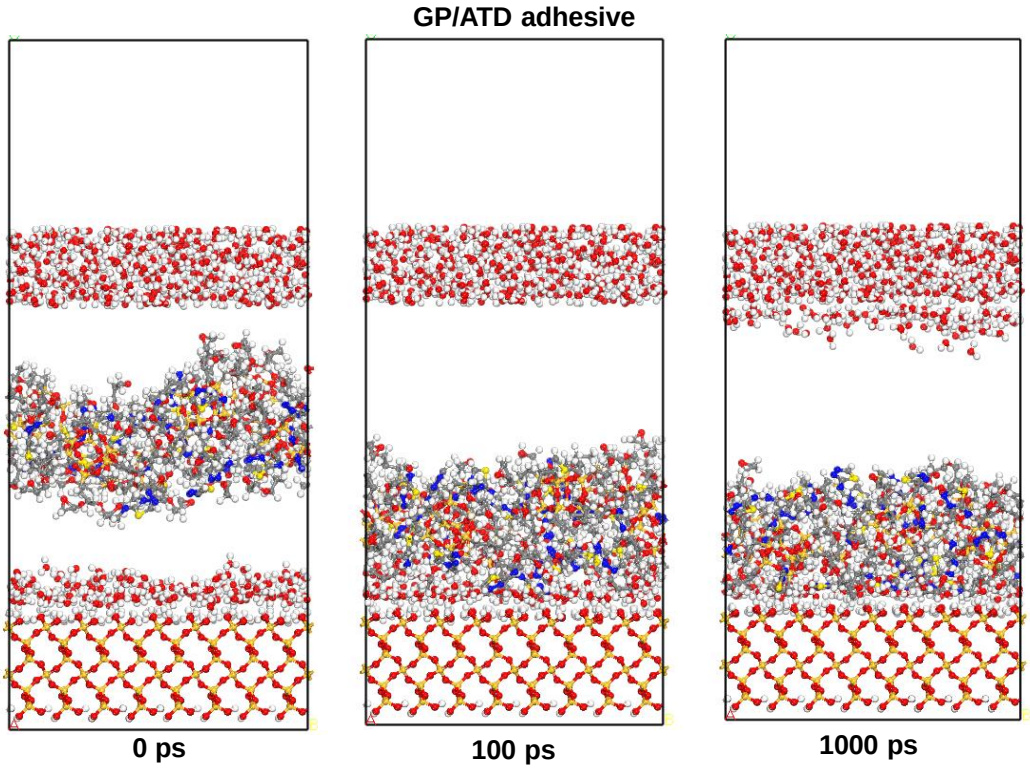

Fig. S12. MD simulations for spatio-temporal dynamics of interfacial adhesion process between the GP/ATD adhesive and glass substrate under water.

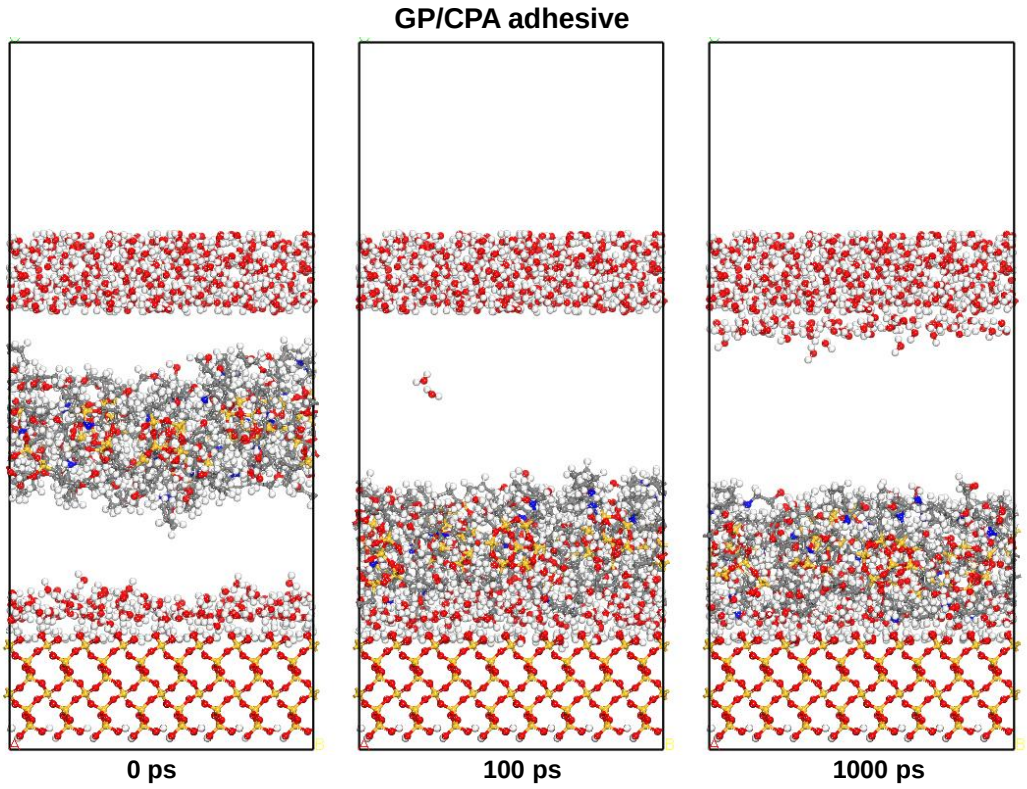

Fig. S13. MD simulations for spatio-temporal dynamics of interfacial adhesion process between the GP/CPA adhesive and glass substrate under water.

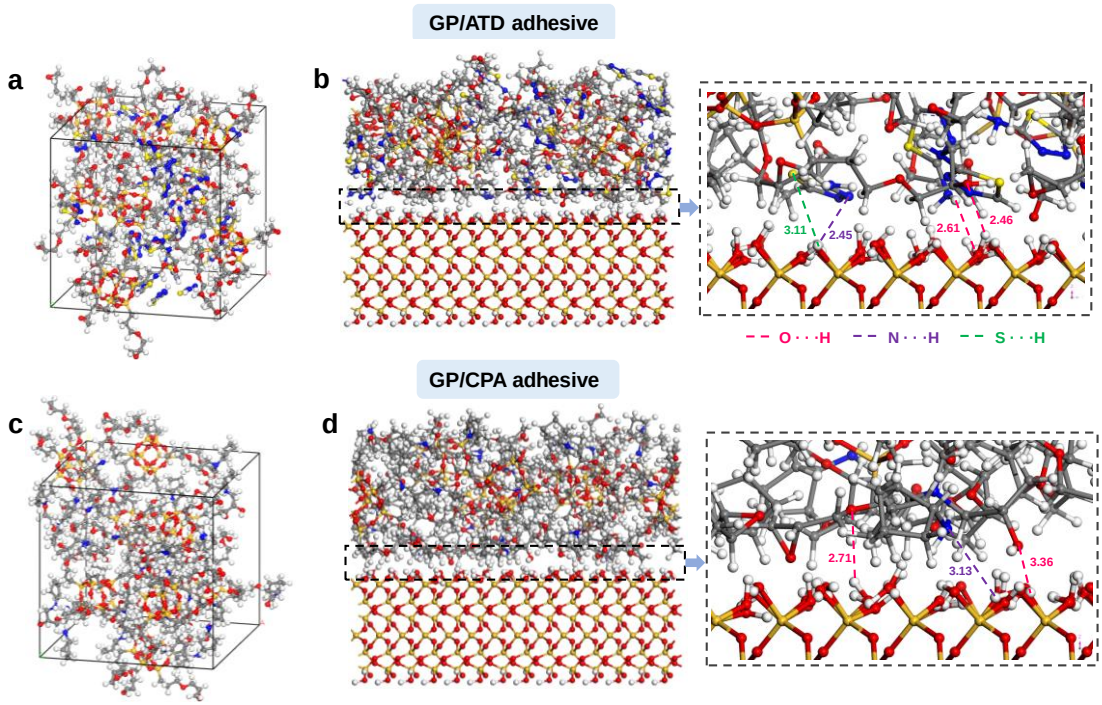

Fig. S14. The most stable conformation with minimum energy of (a) GP/ATD and (c) GP/CPA adhesives. The conformational adhesion state at 1000 ps and the representative interfacial H-bonding interactions of (b) GP/ATD and (d) GP/CPA adhesives to glass substrate in water. It is noted that the water molecules are hidden in the figures for clarity and the unit of interatomic distance is Å.

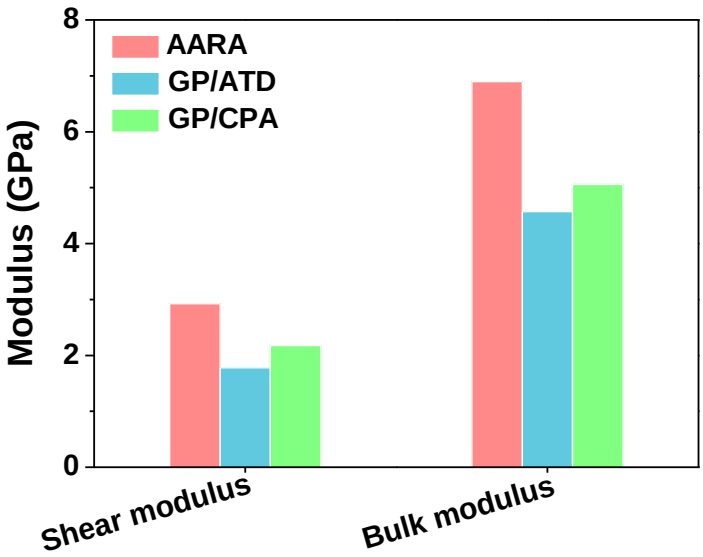

Fig. S15. Calculated shear and bulk modulus of AARA, GP/ATD, and GP/CPA adhesives.

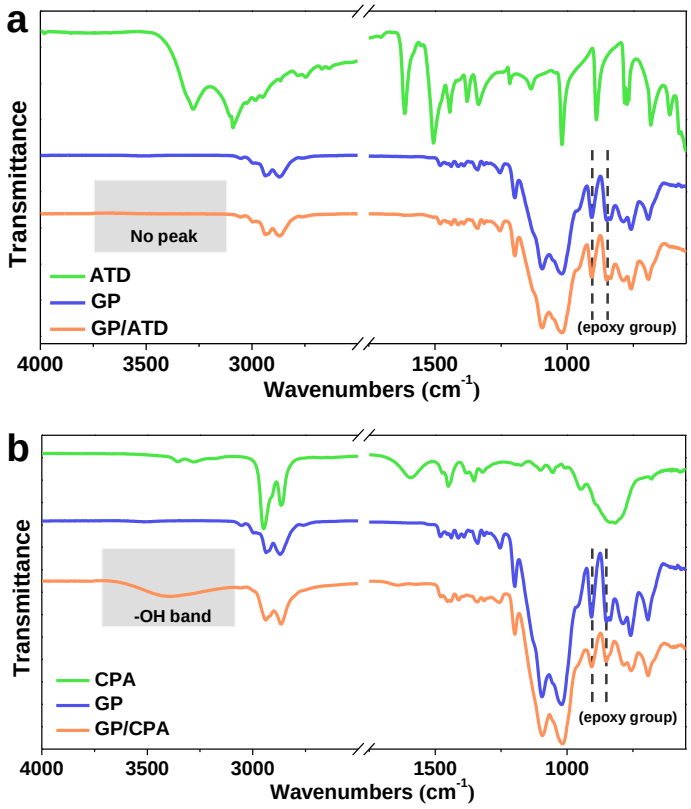

Fig. S16. ATR–FTIR spectra of (a) ATD, GP, and GP/ATD adhesive, and (b) CPA, GP, and GP/CPA adhesive.

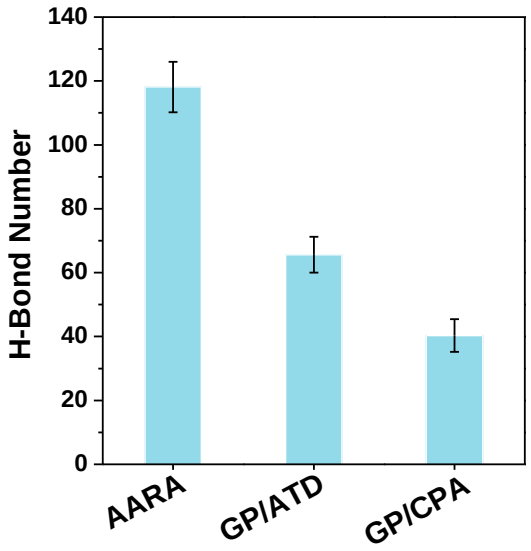

Fig. S17. Calculated hydrogen-bond numbers of AARA, GP/ATD, and GP/CPA adhesives to glass substrate.

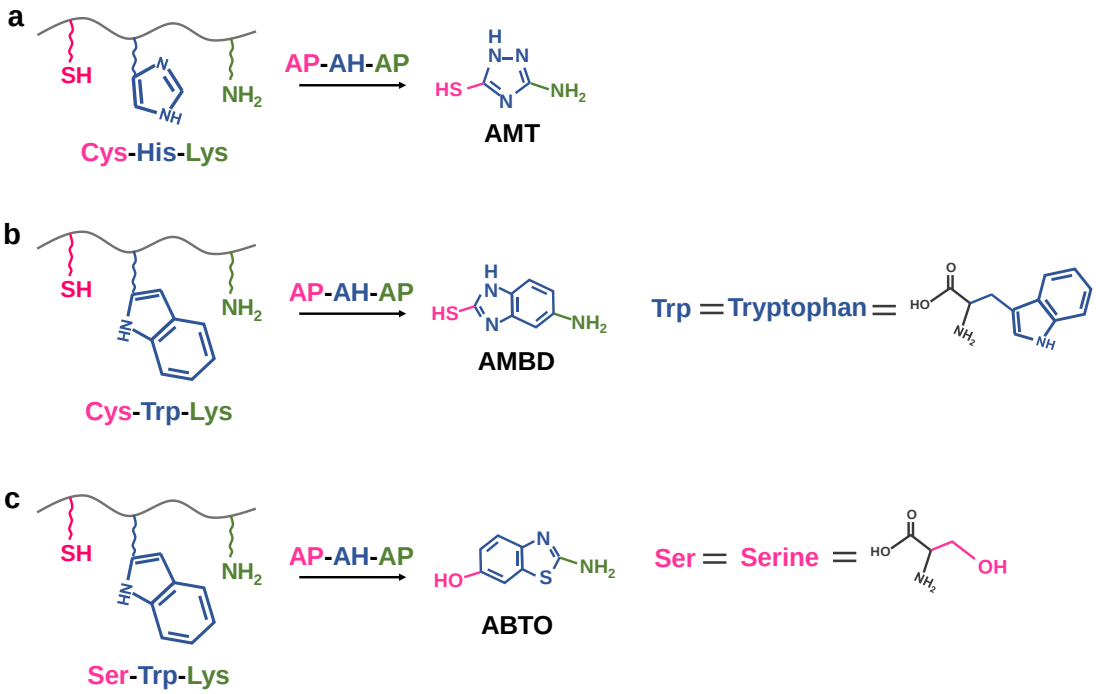

Fig. S18. Schematic illustration of a series of functional blocks with AP-AH-AP group sequence, including (a) AMT, (b) AMBD, and (c) ABTO, reminiscent of the residue combination of Cys-His-Lys, Cys-Trp-Lys, Ser-Trp-Lys, respectively.

Fig. S19. Surface contact angle images of the water droplet to (a) SPGE, (b) DGLA, and (c) BCED layers in air.

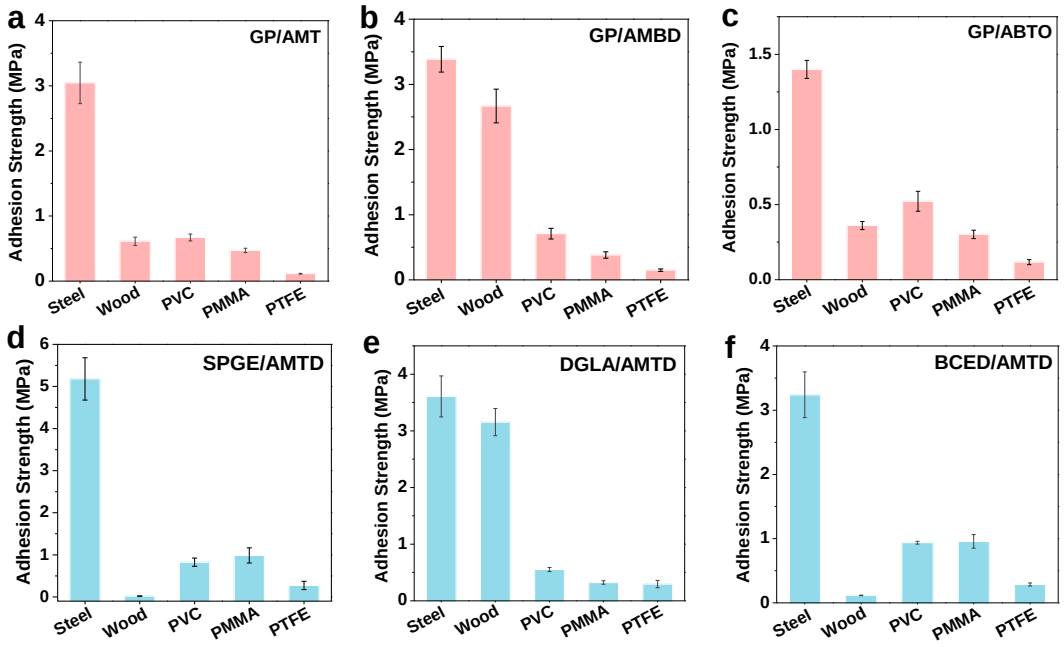

Fig. S20. Lap-shear underwater adhesion strengths of other AARAs, including (a) GP/AMT, (b)GP/AMBD, (c) GP/ABTO, (d) SPGE/AMTD, (e) DGLA/AMTD, and (f) BCED/AMTD adhesives to glass substrates with 48h immersing time at room temperature.

Table S1. Conversion of AARA, GP/ATD and GP/CPA combinations calculated by FTIR.

Sample	Conversion (%)
AARA	88.25
GP/ATD	9.06
GP/CPA	68.75

Table S2. Comparison of the adhesion strength of AARA and other underwater adhesives.

References	**Adhesive type**	**Adhesion strength to glass (MPa)**
This work	**AARA**	**3.92**
Commercial adhesive	Epoxy adhesive	1.54
Commercial adhesive	Polyurethane adhesive	2.17
Commercial adhesive	Silane-modified polyether adhesive	2.01
Mater. Horiz. 2021,8, 2199-2207	Catechol adhesive	0.0027
Adv. Mater. 2019, 31(49): 1905761	Catechol adhesive	0.205
Nat. Commun. 2022, 13(1): 1-9	Catechol adhesive	2.5
ACS Appl. Mater. Interfaces 2020, 12, 18, 20933–20941	Catechol adhesive	0.056
Chem. Eng. J. 2021, 404: 127069	Catechol adhesive	0.0732
Chem. Eng. J. 2022, 430: 133017	Catechol adhesive	0.241
Macromol. Rapid Commun.2019, 40, 1800758	Polyelectrolyte adhesive	0.0809
ACS Sustainable Chem. Eng. 2019, 7, 4, 4508–4514	Polyelectrolyte adhesive	0.1223
Adv. Funct. Mater. 2021: 2109144	Polyelectrolyte adhesive	0.4
Adv. Funct. Mater. 2020, 30(7): 1907064	Hydrophobic adhesive	0.019

Science Advances, 2022, 8(20): eabm9744.	Hydrophobic adhesive	0.216
Adv. Funct. Mater., 2022, 32(2): 2105464	Cation-π adhesive	1
Adv. Funct. Mater., 2021, 31(11): 2009334	Cation-π adhesive	0.185
J. Mater. Chem. A, 2021,9, 12988-13000	Supramolecular adhesive	0.2971
Small, 2020, 16(43): 2004132	Supramolecular adhesive	0.0576
Angew. Chem. Int. Edit. 2017, 129(30): 8857-8861	Supramolecular adhesive	0.0158
Adv. Funct. Mater. 2018, 28(23): 1800599	Supramolecular adhesive	0.00378
Adv. Funct. Mater. 2021, 31(48): 2104296	Supramolecular adhesive	0.066
J. Am. Chem. Soc. 2020, 142(11): 5371-5379	Supramolecular adhesive	1.562
Mater. Horiz., 2022,9, 1984-1991	Supramolecular adhesive	5.15
Adv. Mater. 2021: 2100962	Poly(ionic liquid)s adhesive	0.3
Adv. Mater. 2021: 2008479	Poly(ionic liquid)s adhesive	0.69
Adv. Funct. Mater., 2022: 2205597	Poly(ionic liquid)s adhesive	0.33457
Adv. Funct. Mater. 2022, 2201919	Poly(ionic liquid)s adhesive	0.84
Mater. Horiz., 2021, 8(7): 2057-2064	Poly(ionic liquid)s adhesive	5.18
Chem. Mater., 2021, 33(22): 8822-8830.	Other adhesive	4.1
ACS Appl. Polym. Mater. 2019, 11(6): 6644-6651.	Other adhesive	0.045
Adv. Funct. Mater. 2019, 29(17): 1900450	Other adhesive	0.0065

Mater. Horiz., 2020,7, 2063-2070	Other adhesive	1
Adv. Mater. Interfaces, 2017, 4(22): 1700506	Other adhesive	0.65
Mater. Horiz., 2020, 7, 282-288	Other adhesive	0.6

Reference

1. G. Lin, J. Yin, Z. Lin, Y. Zhu, W. Li, H. Li, Z. Liu, H. Xiang and X. Liu, *Prog. Org. Coat.*, 2021, **156**, 106269.